Estudios Geológicos
julio-diciembre 2022, 78(2), e147
ISSN-L: 0367-0449
https://doi.org/10.3989/egeol.44641.614

Remote sensing and GIS-based mining prospection of Fe-Mn-Pb oxide mineralisation at Jbel Skindis (Eastern High Atlas, Morocco).

Prospección minera de la mineralización de óxidos de Fe-Mn-Pb en Jbel Skindis (Alto Atlas Oriental, Marruecos) basada en teledetección y SIG

Adnane Tobi[1,2,*], Mourad Essalhi[1], Daoud El Azmi[2], Mostapha Bouzekraoui[1,3], Bilal El Ouaragli[2]

1: Moulay Ismail University, Faculty of Sciences and Techniques, Applied Geology Laboratory, M.B. 509, Boutalamine, Errachidia, Morocco. ORCID ID: https://orcid.org/0000-0001-7640-6785, https://orcid.org/0000-0001-5696-9636.
2: Africorp Mining Company, Africorp Consortium group, Casablanca, Morocco. ORCID ID : https://orcid.org/0000-0001-5785-6596, https://orcid.org/0000-0002-0590-5488.
3: Mohammed V University in Rabat, Faculty of Sciences, Geosciences, Water, Environment Laboratory, Morocco. ORCID ID: https://orcid.org/0000-0002-5060-3585.
* Corresponding author: tobi.adnane@gmail.com

Abstract

In recent years, remote sensing has had a prominent place in mineral exploration programs given its potential to identify alteration minerals, such as clay and hydroxyl minerals. Those minerals represent significant guides to mineral deposits considering their potential to host valuable concentrations of base metal elements. This work focuses on Fe-Mn-Pb mineral deposits within the Jbel Skindis area as a case study to illustrate the application of remote sensing images and GIS systems to highlight prospective zones and to extract information on ore-controlling factors using image enhancement and integration methods. Field observations and XRD data showed that the main remotely sensed alteration anomalies are characterized by oxides and hydroxides. Based on those indicative minerals, a mapping using Aster L1T and Landsat 8 OLI data was done: the 5/4 ratio highlighted gossans zones and the RGB combination (4/6, 2/1, 3/2) accentuates the hydrothermally altered areas. The lineament map extracted from Sentinel 2A and Landsat imagery allowed the reconstitution of the megafracture network that affected the region. The multi-criteria analysis of these satellite-derived data along with available geological data outcomes to delineate prospective zones in the study area, were found to be in highly fractured areas developing gossans and Fe rich alteration. Verified via field survey, this approach was successfully applied to the Jbel Skindis area to rapidly delineate oxidized ore outcrops. This provides a remote sensing model for future prospecting efforts for similar mineral deposits both in the Eastern High-Atlas province and in other similar areas.

Keywords: Remote sensing; Fe-Mn-Pb deposits; Multicriteria analysis; Mineral exploration; Eastern High-Atlas.

Recibido el 21 de marzo de 2022; Aceptado el 16 de octubre de 2022; Publicado online el 21 de noviembre de 2022

Citation / Cómo citar este artículo: Tobi, A. et al. (2022) Remote sensing and GIS-based mining prospection of Fe-Mn-Pb oxide mineralisation at Jbel Skindis (Eastern High Atlas, Morocco). Estudios Geológicos 78(2): e147. https://doi.org/10.3989/egeol.44641.614

Resumen

En los últimos años, la teledetección ha ocupado un lugar destacado en los programas de exploración minera dada su utilidad para identificar minerales de alteración, como la arcilla y los hidróxidos. Estos minerales son guías significativas para encontrar depósitos minerales que albergan concentraciones valiosas de metales base. Este trabajo se centra en las mineralizaciones de Fe-Mn-Pb dentro del área de Jbel Skindis consideradas como un zona de estudio para ilustrar la aplicación de imágenes de teledetección y de un sistema SIG para delinear zonas de interés para la exploración minera y extraer información sobre los factores que controlan las concentraciones de metales utilizando tratamiento de datos satélites e integración de imágenes. De acuerdo con las observaciones de campo y los datos DRX las principales anomalías de alteración deducidas del tratamiento de datos satélite se caracterizan por óxidos e hidróxidos. En base a estos minerales, se realizó un mapeo utilizando los datos de Aster L1T y Landsat 8 OLI: la relación 5/4 resalta las zonas de Gossans mientras la combinación RGB (4/6, 2/1, 3/2) señala las áreas alteradas. El mapa de lineamientos extraído de las imágenes de Sentinel 2A y Landsat permitió reconstituir la red de megafracturas que afectó a la región. El acoplamiento entre un análisis multi-criterio de los datos derivados de satélites y los datos geológicos disponibles, permitió delinear zonas de interés para la exploración minera en el área de estudio. Estas zonas corresponden a áreas altamente fracturadas en las cuales se desarrollan gossans y alteración rica en Fe. Este enfoque junto con un control a través de un estudio de campo, se aplicó con éxito en el área de Jbel Skindis para delinear rápidamente los afloramientos de mineralizaciones oxidadas. Esto proporciona un modelo de teledetección para futuros esfuerzos de prospección de depósitos minerales similares tanto en la provincia oriental del Alto Atlas como en otras áreas similares.

Palabras clave: Teledetección; Yacimientos de Fe-Mn-Pb; Análisis multi-criterio; Exploración mineral; Alto Atlas Oriental.

Introduction

The Jbel Skindis Mountain is one of the important morphogeological features of the eastern High Atlas in Morocco; it's located at 15km in the NNE of Talsint city. This region contains several polymetallic base metal deposits (Fe, Mn, Pb, Cu with various amount of Zn and Ba). The ore deposits consist of massive bodies known as replacement ore bodies, and minor veins of lead sulfides and carbonates hosted by dolomitic limestone. The economic importance of this region has prompted the realization of some detailed geological studies (Bouchta, 1967; Caïa, 1969, 1976; Haddoumi, 1998; Mouguina, 2004; Choulet *et al*., 2014; Bouabdellah & sangster, 2016), but little attention was given to the polymetallic ore deposits.

Remote sensing is a valuable tool in mineral exploration, data gathered through sensors can be used in the strategic phase to explore large region, reducing by the way the time and the exploration costs. Multispectral imaging data have been successfully used for mineral exploration to map hydrothermal alteration zones in arid and semi-arid regions. Several recent studies used satellite data in the exploration of sediment-hosted mineralization around the world (e.g., Molan & Behnia, 2013; Yang *et al*., 2018; Ghorbani *et al*., 2019; Sekandari *et al*., 2020). In this study, we will utilize multi-sensor satellite data processing and GIS system to highlight prospective areas associated with Fe-Mn-Pb mineral resources in the Jbel Skindis. This region presents a favorable site for remote sensing analysis due to its semi-arid climate with a very low vegetation cover and well-exposed bedrock.

The employed methodology includes two steps: first (i) we applied various image processes (Principal Component Analysis (PCA), Band ratios, image filtering and color composite) on a data from Landsat 8 OLI, Sentinel 2A and Aster L1T sensors in order to map lineaments and alteration minerals, then (ii) the resulted data was integrated and analyzed in a GIS system to establish mining prospecting guides, allowing targeting potential areas to be explored in the tactical phase.

Geological setting

The High Atlas corresponds to an intra-continental belt (Mattauer *et al*., 1977), bounded by the Variscan Meseta and the High Plateau to the north, and the Precambrian Anti-Atlas massif with its Paleozoic cover to the south (Figure 1). It is made up of a Mesozoic and Cenozoic folded cover, which overlies a Paleozoic basement consolidated during the Variscan orogenesis (Piqué & Michard, 1989). The Jbel Skin-

dis is an anticline structure striking NE-SW, extending over 25 km, which lies near the northern edge of the Eastern High Atlas (Figure 1). The stratigraphic series start with conglomerate, red claystone, and basalt of the Triassic age (Bouchta, 1967), unconformably superimposed by Jurassic formations: (i) The Liassic includes dolostone, limestone and marls. (ii) The Middle Jurassic is essentially represented by green marl and limestone followed by claystone and sandstone (Dresnay, 1963). The Cretaceous formations contain an alternation of conglomerate, sandstone and claystone, followed by versicolor marls and limestone beds with nodular chert (Haddoumi, 1998).

The Eastern High-Atlas is a metallogenic province exhibiting many base metal mineralization as Mississippi Valley-Type Pb-Zn deposits (MVT) (Jbel Bou Dhar, Jbel Houanite, Jbel Bou Arhous, ...) (Choulet *et al*., 2014), and sedimentary hosted Pb-Cu deposit (Anoual, Bou Sellam, …) (Caïa, 1969). The Zn-Pb-Cu ore deposits of the Moroccan High Atlas belong to the Zn-Pb province of the circum-Mediterranean Sea and Alpine Europe (Rouvier *et al*., 1985). Previous studies conducted on Pb-Zn ore deposits of the Eastern High-Atlas reported two ore morphologies (Emberger, 1965; Mouguina, 2004; Bouabdellah & Sangster, 2016): (i) the Lower Jurassic stratiform lenses of Zn-Pb-Fe sulfides and (ii) the Middle Jurassic Zn-Pb sulfide ores disseminated in gabbro, and filling veins in calcareous host rocks.

Based on a field survey in the Boumaadine area, we provide a first preliminary description of the polymetallic deposits in the Jbel Skindis area. Those deposits are hosted by dolomitic limestone of the Lower Jurassic age. Ore minerals consist mainly of Fe-Mn-Pb oxides with less amount of sulfides, they

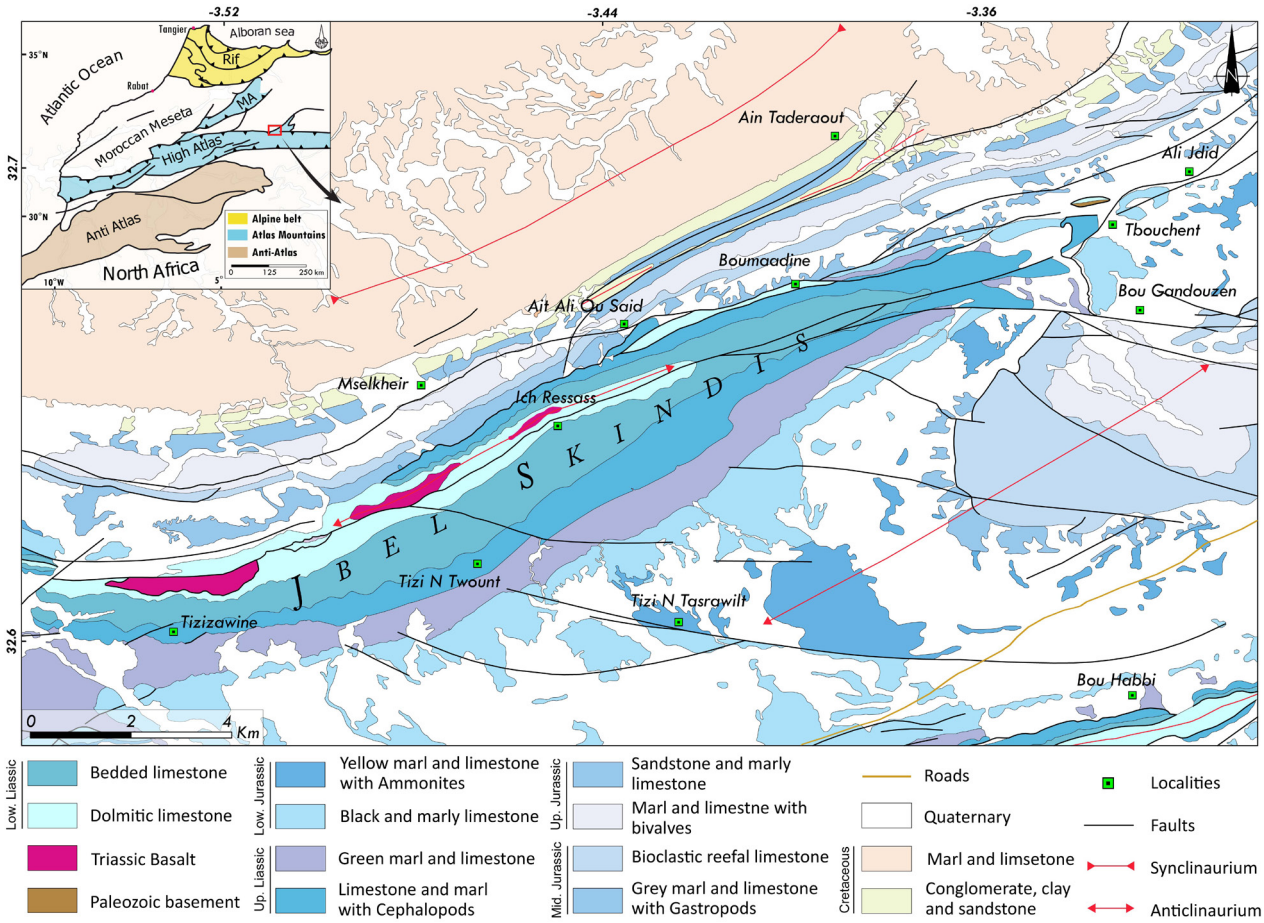

Figure 1.— Geological map of Jbel Skindis area, extracted from the geological maps of Talsint and Mazzer at 1:50000 (Haddoumi et al., 2018. 2019).

occur as metric discordant lenses, disseminated or as filling of fractures of various dimensions and directions (Figure 2). Petrographic study and XRD analysis carried out in the Boumaadine area allowed us to distinguish a mineralogical assemblage consisting mainly of coronadite, hematite, plumboferrite, mag-

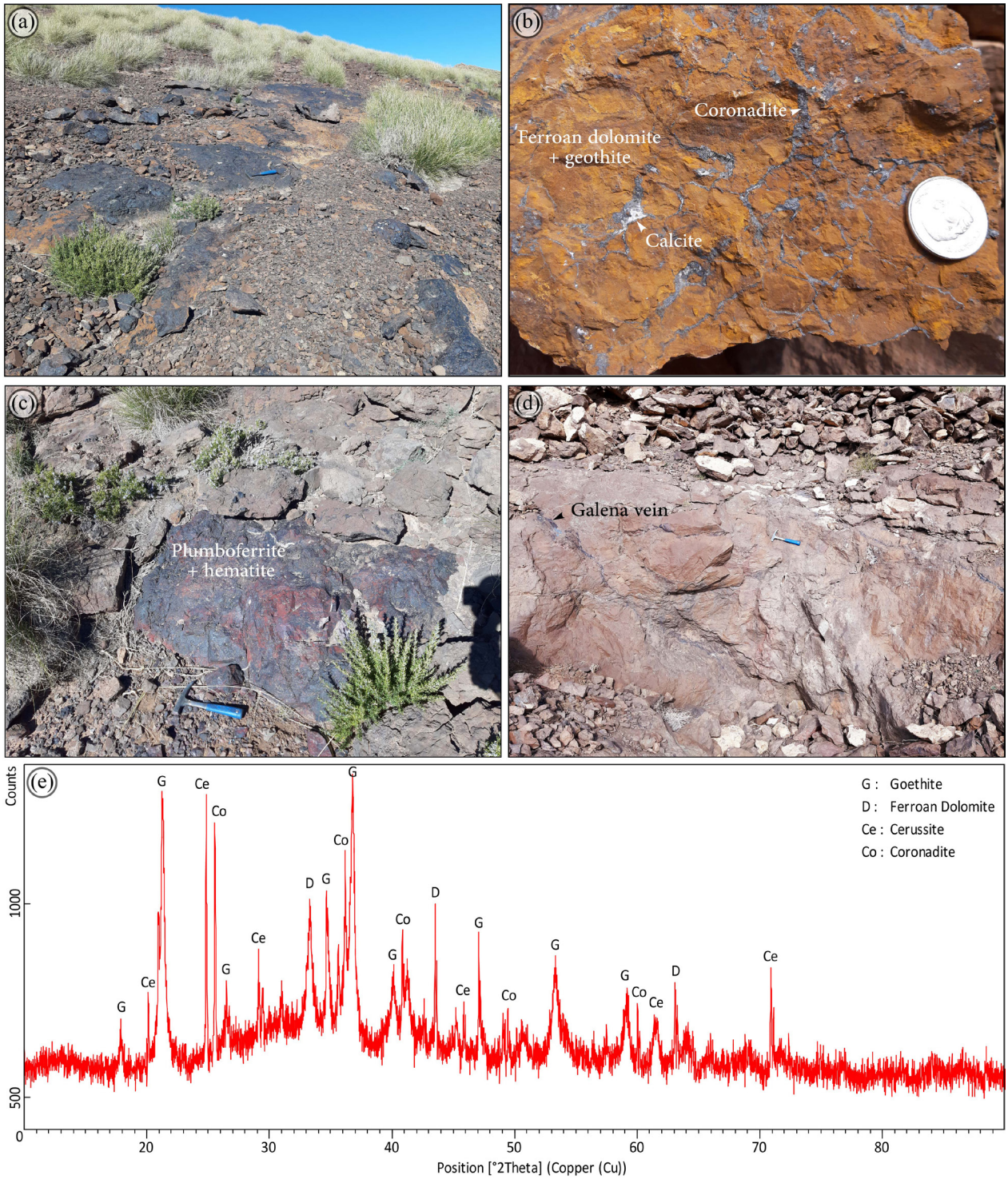

Figure 2.— (a) Gossan outcrop. (b) Coronadite and calcite veinlets hosted by hydrothermally altered dolostone. (c) Massive plumboferrite and hematite lens. (d) Galena vein. (e) XRD spectra of a Fe-Mn-Pb oxide ore sample.

netoplumbite, galena, chalcopyrite, cerussite and calcite.

Dolomitization and hematitization are the main types of alterations observed in the host rock. The development of alteration is mainly controlled by the permeability of the surrounding rock, and by fractures, joint fissures. The altered zones extend over decametric extensions, which allowed their mapping using satellite images with a spatial resolution of 15 and 30 m. Alteration minerals associated with the orebodies consist of ferroan dolomite, goethite, hematite and limonite (Figure 2). These index minerals were considered as the mineralized zone indicators on the satellite images.

Materials and methods

Used data and pre-processing

In this study, multi-sensor satellite images were used (Sentinel 2A, Aster L1T and Landsat 8 OLI). They have been captured in very low cloud cover and present excellent image quality (Table 1). These images have been assigned to Lambert Conform Conic projection, Merchich datum.

The Advanced Spaceborne Thermal Emission and Reflection Radiometer (ASTER), Level 1 precision terrain corrected registered at-sensor radiance data (L1T) contains calibrated at-sensor radiance that has been geometrically corrected and rotated to a north-up UTM projection. The ASTER_L1T comprises 14 frequency bands; visible and near infrared (VNIR) frequencies with three bands at 15-meter resolution, short-wave infrared (SWIR) frequencies with six bands at 30-meter resolution, and thermal infrared (TIR) wavelength with five bands at 90-meter resolution (Duda et al., 2015) (Table 2). In this study we used a scene image acquired on September 26, 2006, downloaded from United States Geological Survey (USGS) website. The Aster scene covering an area of

Table. 1.— Multispectral images used in this work.

Data	Source	Level	Acquisition date	Scene cloud cover
ASTER	USGS https://earthexplorer.usgs.gov	1T	2006/09/26	Cloud-free
Landsat 8 Oli	EOS https://eos.com/landviewer/?s=Landsat8	L1-T1	2020/07/22	1.07%
Sentinel 2A	ASF DAAC https://vertex.daac.asf.alaska.edu	1C	2019/07/15	Cloud-free

Table 2.— Description of the Sentinel-2A, Landsat 8 Oli, and Aster sensors.

Sentinel-2A			OLI			ASTER		
Band	Central Wavelength (nm)	Spatial Resolution (m)	Band	Central Wavelength (nm)	Spatial Resolution (m)	Band	Central Wavelength (nm)	Spatial Resolution (m)
1	0.4430	60	1	0.4430	30	1	0.5560	15
2	0.4900	10	2	0.4826	30	2	0.6610	15
3	0.5600	10	3	0.5613	30	3N	0.8070	15
4	0.6650	10	4	0.6546	30	4	1.6560	30
5	0.7050	20	5	0.8646	30	5	2.1670	30
6	0.7400	20	6	1.6090	30	6	2.2080	30
7	0.7830	20	7	2.2010	30	7	2.2660	30
8	0.8420	10	8	0.5917	15	8	2.3360	30
8A	0.8650	20	9	1.3730	30	9	2.4000	30
9	0.9450	60	10	10.9000	100	10	8.2910	90
10	1.3750	60	11	12.0000	100	11	8.6340	90
11	1.6100	20				12	9.0750	90
12	2.1900	20				13	10.6570	90
						14	11.3180	90

60 x 60 km was first corrected from atmospheric effect using the Fast Line-of-sight Atmospheric Analysis of Hypercubes (FLAASH) algorithm. Then, all bands were resampled to 30 m resolution using the nearest neighbor resampling method and regrouped in one multispectral image.

Landsat 8 OLI data products are generated from Landsat 8 Operational Land Imager (OLI) and Thermal Infrared (TIRS) sensors. The images used in this work (Level-1, Tier 1), acquired from the Earth Observing System (EOS) website, represent the highest available data quality; they are radiometrically calibrated and orthorectified using ground control points (GCPs) and digital elevation model (DEM) (Ihlen, 2019). The data consists of nine spectral bands with a spatial resolution of 30 meters for VNIR and SWIR bands (1 to 7) and the Cirrus band (9). The resolution for band 8 (panchromatic) is 15 meters. Thermal bands 10 and 11 are collected at 100 meters (Roy *et al*., 2014) (Table 2). In this work, only the VNIR and SWIR bands were grouped into a single multispectral image with a resolution of 30 m, corrected from atmospheric effect using FLAASH algorithm, then spatially enhanced by combination with the panchromatic band at 15 m spatial resolution

The Sentinel 2A comprises multi-spectral data with 13 bands in the visible, near infrared, and short-wave infrared part of the spectrum, with four bands at 10 m spatial resolution, six bands at 20 m, and three bands at 60 m (Drusch *et al*., 2012) (Table 2). The level-1C images downloaded from Alaska Satellite Facility Distributed Active Archive Center (ASF DAAC) include radiometric and geometric corrections (ortho-rectification and spatial registration on a global reference system with sub-pixel accuracy). The cloudless images covering the study zone were resampled to 10 m resolution using the nearest neighbor method and regrouped in one multispectral image.

Image processing methodology

As shown in Figure 3, the used method is as follows: in the first step, alteration minerals were mapped from Aster and Landsat enhanced images using bands ratio and false colors composite. In the second step, a fracturing map was obtained from Sentinel and Landsat images. And in the last step, the data derived from processing remote sensing images and field data were integrated into a GIS system and analyzed to set up mining prospecting guides.

Mineral alteration mapping

Iron oxide, clay and carbonate minerals associated with hydrothermally altered or weathered rocks have been investigated by many authors using band ratios (Pour *et al*., 2010; Khunsa *et al*., 2017; Yang *et al*., 2018). Ratios enhance the contrast between materials with different reflectance at specific wavelengths and suppress the effects of shadows (topography) (Prost, 2013).

Spectral reflectance of a rock mainly depends on its mineralogical composition, which produces characteristic absorption features in different wavelength of the electromagnetic spectrum (Younis *et al*., 1997). The ferrous iron (Fe^{2+}) produces absorptions troughs at about 0.45, 1.0-1.1, 1.8-1.9, and 2.2-2.3 µm, and the ferric iron (Fe^{3+}) is characterized by absorptions troughs at about 0.65 and 0.87 µm (Figure 4) (Rajendran *et al*. 2011).

The superficial part of an ore deposit, highly oxygenated and hydrated due to the combined actions of the atmosphere and biosphere is known as Gossan (Jébrak MI, 2008). The main products of weathering are typically ferric oxides and hydroxides expressed by goethite, jarosite and hematite. Other important associated minerals are clay minerals, gypsum and silica (e.g. Atapour & Aftabi 2007; Essalhi *et al.*, 2011).

According to (Başıbüyük & Ekdur, 2018) gossan zones are highlighted on the obtained images using 4/3 band ratio of Landsat TM. Given that we used Landsat 8 data in this study, the equivalent band ratio 5/4 was used to detect gossan zones.

Both band rationing and band composite techniques can also be used to detect natural resources basing on VNIR and SWIR bands. As suggested by Erdas, 2007, the Aster hydrothermal composite of the BR 4/6, 2/1 and 3/2 was used to highlight altered rocks characterized by both iron bearing and hydroxyl minerals.

Lineament extraction

The linear geological discontinuities (lineaments) that interest us in this study are structural elements

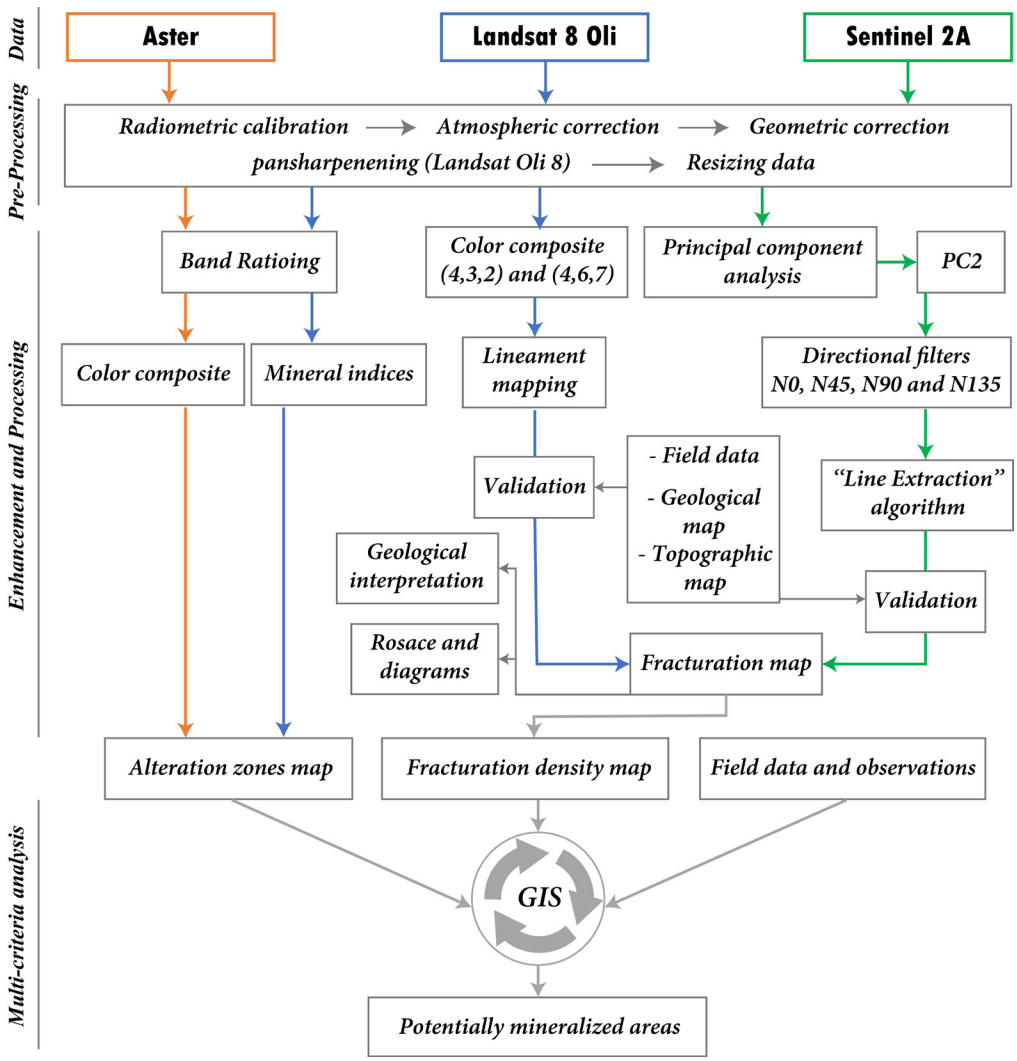

Figure 3.— Flowchart of satellite image processing methodology.

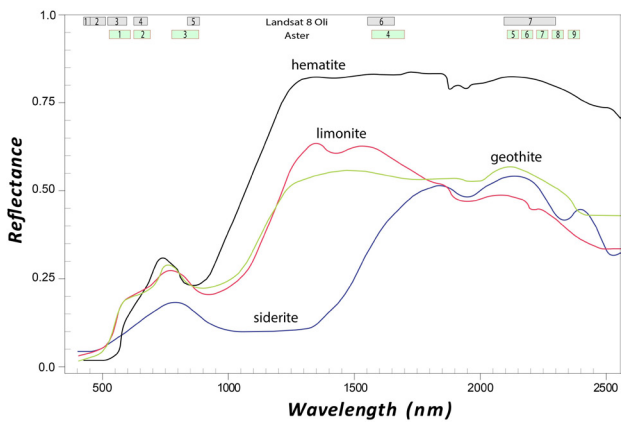

Figure 4.— Spectral profile showing the main absorption features of some iron minerals (hematite, limonite, goethite and siderite (spectra from USGS spectral library)).

such as faults and fractures. The identification of the lineaments in the study area was carried out in two steps; (i) firstly a manual extraction of the lineaments was done by visual analysis of the Landsat 8 OLI images, afterward, (ii) an automated lineament extraction was performed on Sentinel data. (iii) Then the lineaments extracted from both satellite imagery were combined in order to draw a synthetic map of fracturing.

i) Visual interpretation:

For the manual extraction of lineaments, we approached a visual analysis on the screen of the Landsat OLI image in RGB false colors composite (4, 6, 7). This triplet band composition was chosen to give

better color composite for visual interpretation, the lineaments highlighted were then manually digitized.

ii) Automatic extraction:

The automatic lineament extraction was performed in order to identify lineaments that are not recognized by visual analysis of the images. The automated lineament extraction was performed in two steps;

(1) We carried out a Principal Component Analysis (PCA) on Sentinel 2A multispectral image; the PCA is an operation that reduces data redundancy and does correlation between initial bands. This process attempts to maximize (statistically) the amount of information from the original data into the least number of new bands, called principal components (PC) (Singh & Harrison, 1985).

(2) We applied directional filters on PC bands with a matrix of 3x3 pixels in the N0, N45, N90 and N135 directions (Table 3), which allows enhancing of lineaments in all directions. After performing many lineament extraction tests, we selected the PC2 band which gave optimal results.

(3) The next step is the extraction of lineaments through the "Line Extraction" algorithm of Geomatica software; this module extracts the linear features from the images and records the lines in vector format by using the six parameters shown in the table 4.

(4) The lineaments were then loaded into GIS software and overlapped on the geological and the topographic maps of Talsint and Mazzer at 1/50000 (Haddoumi *et al*., 2018; Haddoumi *et al*., 2019); this operation allowed us to validate the lineament map and to remove the lineaments that coincide with rivers, roads, geological contours and cliffs. In the last step the lineament extracted manually and automatically were combined to obtain a synthetic map of lineament.

Multi-criteria analysis

This process was performed in order to optimize the data interpretation; it involves the combining of data from multiple sources to create synergies that allows revealing new information (Scanvic, 1993). We approached the multicriteria analysis by integrating the data derived from the processing of satellite images (lineaments and mineral alteration zones) and field surveys data into a GIS system. That leads revealing ore controlling factor and setting up prospecting guides that allows identifying potentially mineralized areas.

Results

Mineral Mapping

Landsat BR 5/4 was used to detect gossan zones. As shown in figure 5, areas with high DN values indicated with bright tones highlight the gossan signature in bright pixels; these later present a NE-SW orientation. We note also that some accentuated signatures coincide with green vegetation zones located in the valley between Ghazwane and Tizizawine, and in Tbouchent area.

Table 3.— Sobel kernel filters in four main directions.

N-S			NE-SW			E-W			NW-SE		
-1	0	1	-1.4142	-0.7071	0	-1	-1	-1	0	-0.7071	-1.4142
-1	0	1	-0.7071	0	0.7071	0	0	0	0.7071	0	-0.7071
-1	0	1	0	0.7071	1.4142	1	1	1	1.4142	0.7071	0

Table 4.— Parameters used for automatic lineament extraction.

Name	Caption	Applied values
RADI	Radius of the edge detection filter	10
GTHR	Threshold for edge gradient	100
LTHR	Threshold for curve length	30
FTHR	Threshold for line fitting error	3
ATHR	Threshold for angular difference	30
DTHR	Threshold for linking distance	35

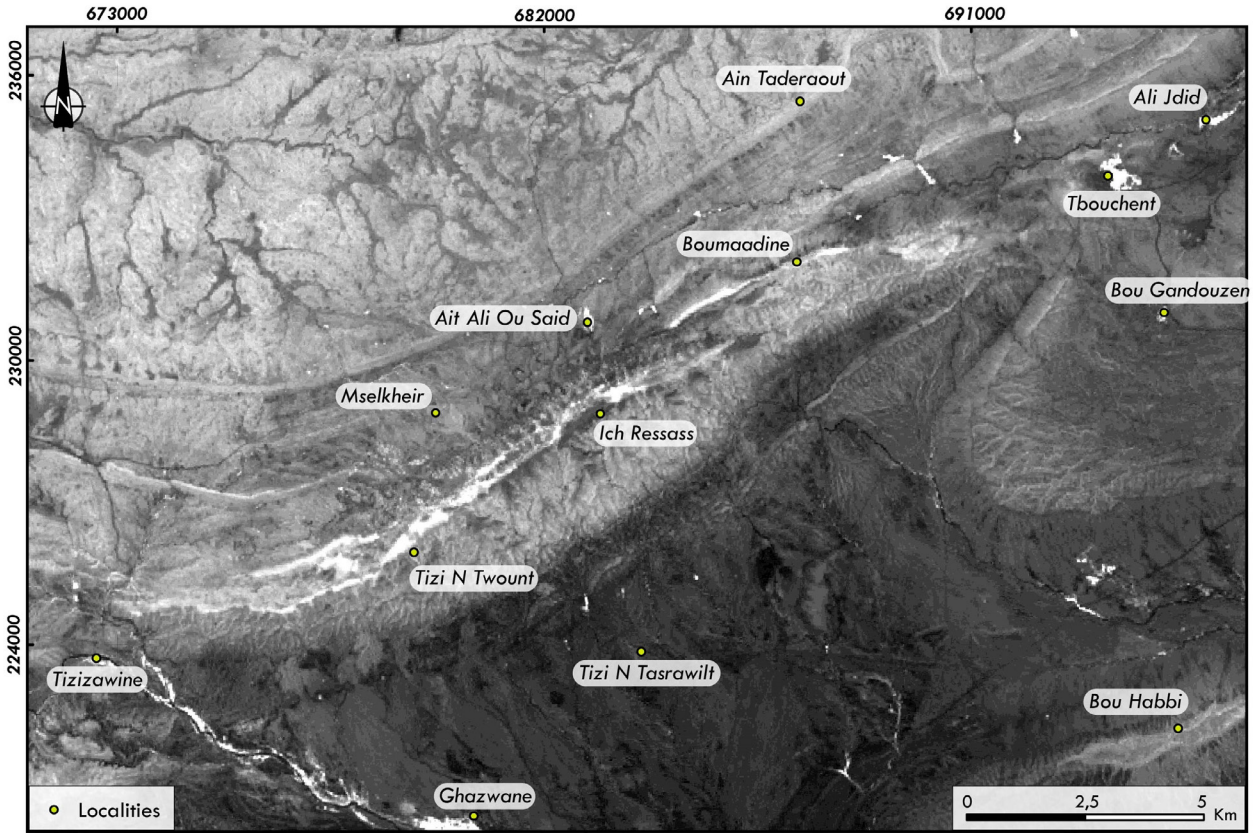

Figure 5.— Gossan ratio (5/4) highlighting Fe rich zones in bright pixels.

Based on the VNIR and SWIR bands of Aster images, a colored composite image was created by the BR 4/6, 2/1 and 3/2. This combination allowed very good differentiation of hydrothermally altered outcrops represented in figure 6 by areas in blue-cyan tones.

Lineaments analysis

The false colors composite (4, 6, 7) of Landsat OLI allows us to highlight structural features. Based on visual analysis and interpretation of this image, we manually digitize the lineaments in the study zone, which leads us to establish a map containing 273 lineaments (Figure 7).

The automated extraction of lineament allowed us to obtain four lineament maps grouping 639 lineaments (Figure 8). The results show an abundance of the NE-SW trending lineaments (41%). The E-W lineaments (26%) are scattered in the study area, whereas the NW-SE ones (24%) are concentrated in the SW part of the study zone, and the N-S lineaments (9%) are subtle and dispersed.

Figure 9 shows the synthetic map of geological fracturing obtained from different processing operations. The map, regrouping 912 lineaments, allows us to have an overview of the fracturing network's geometry; the lineaments appear preferentially between Tizizawine and Ali Jdid regions, and they are scattered in the SE part of the study zone. The lineament's orientation rose diagram show the predominance of the ENE-WSW oriented lineaments.

The lineament density indicates the concentration of lineaments per surface (Hung *et al.*, 2005). Within the present work, this parameter is employed to spot areas with strong fracturing. The lineament density map (Figure 10) shows high fracturing intensities within the areas of Boumaadine, Tbouchent and Ich Ressass, located on the axis of Jbel Skindis, and around Bou Habbi and Tizizawine areas.

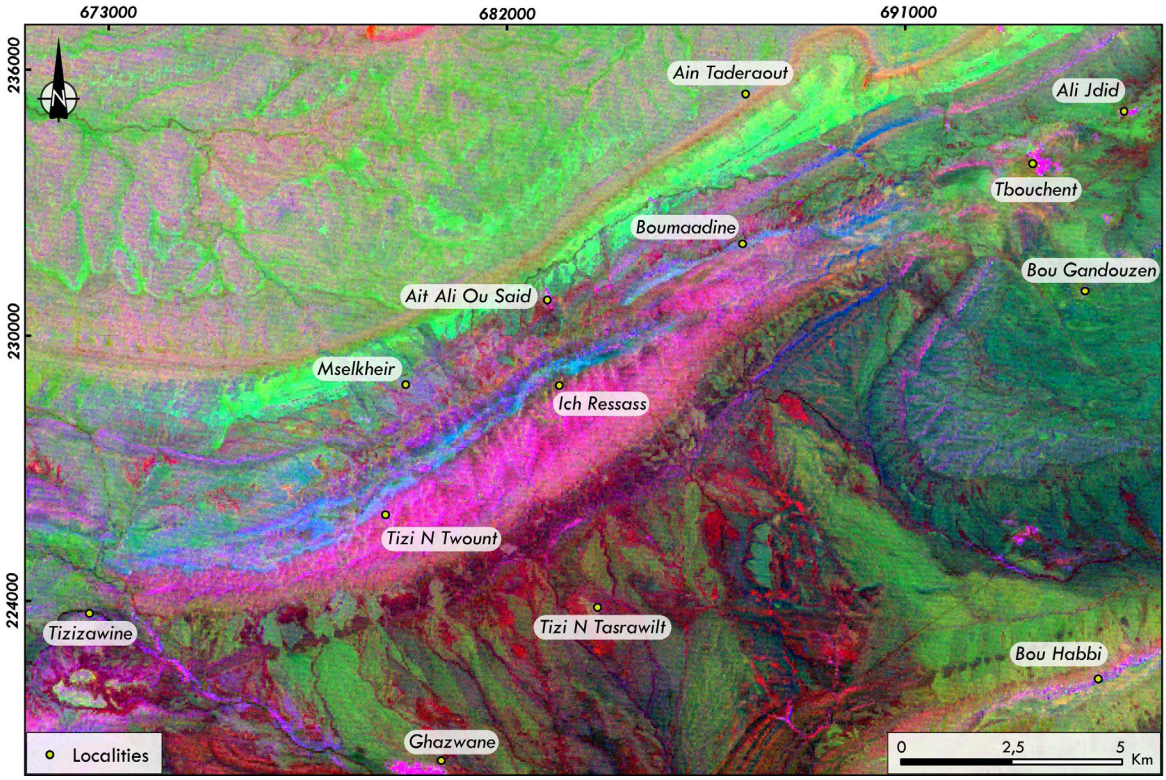

Figure 6.— False colors composite image (4/6, 2/1, 3/2) highlighting hydrothermally altered areas in blue-cyan tones.

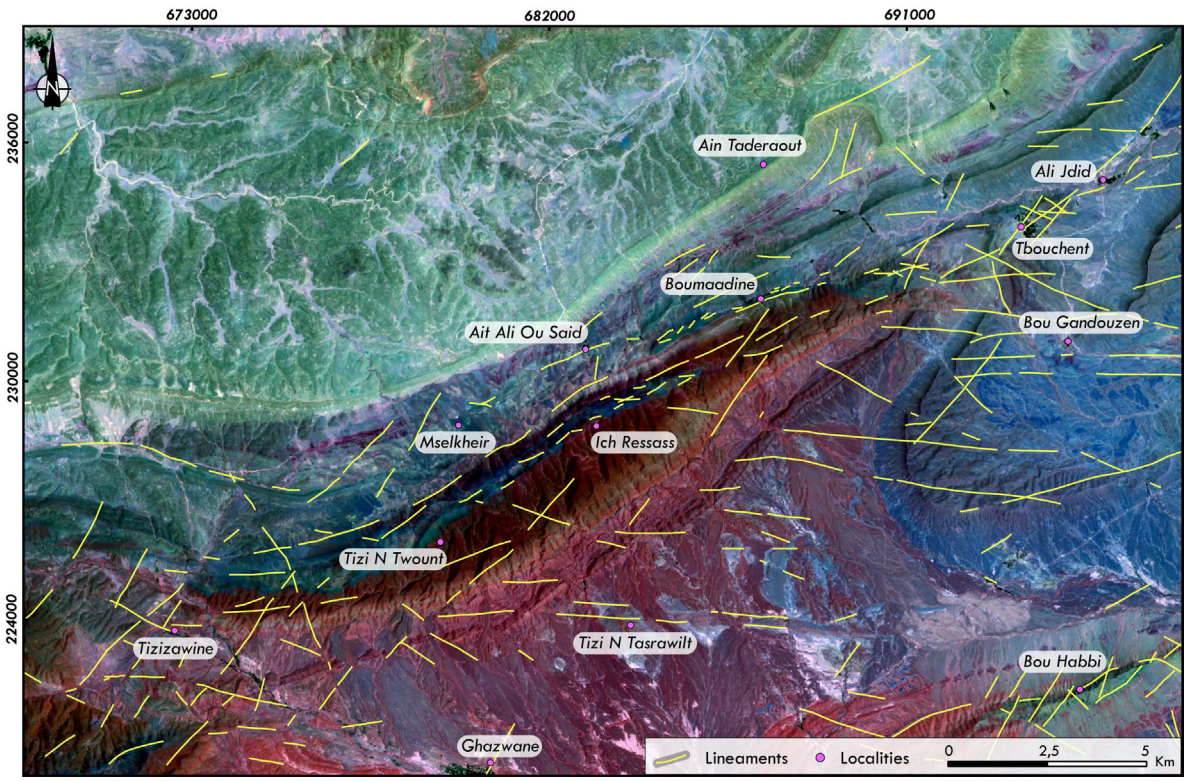

Figure 7.— Map of fractures extracted manually from the false colors composite image (4, 6, 7) of Landsat OLI.

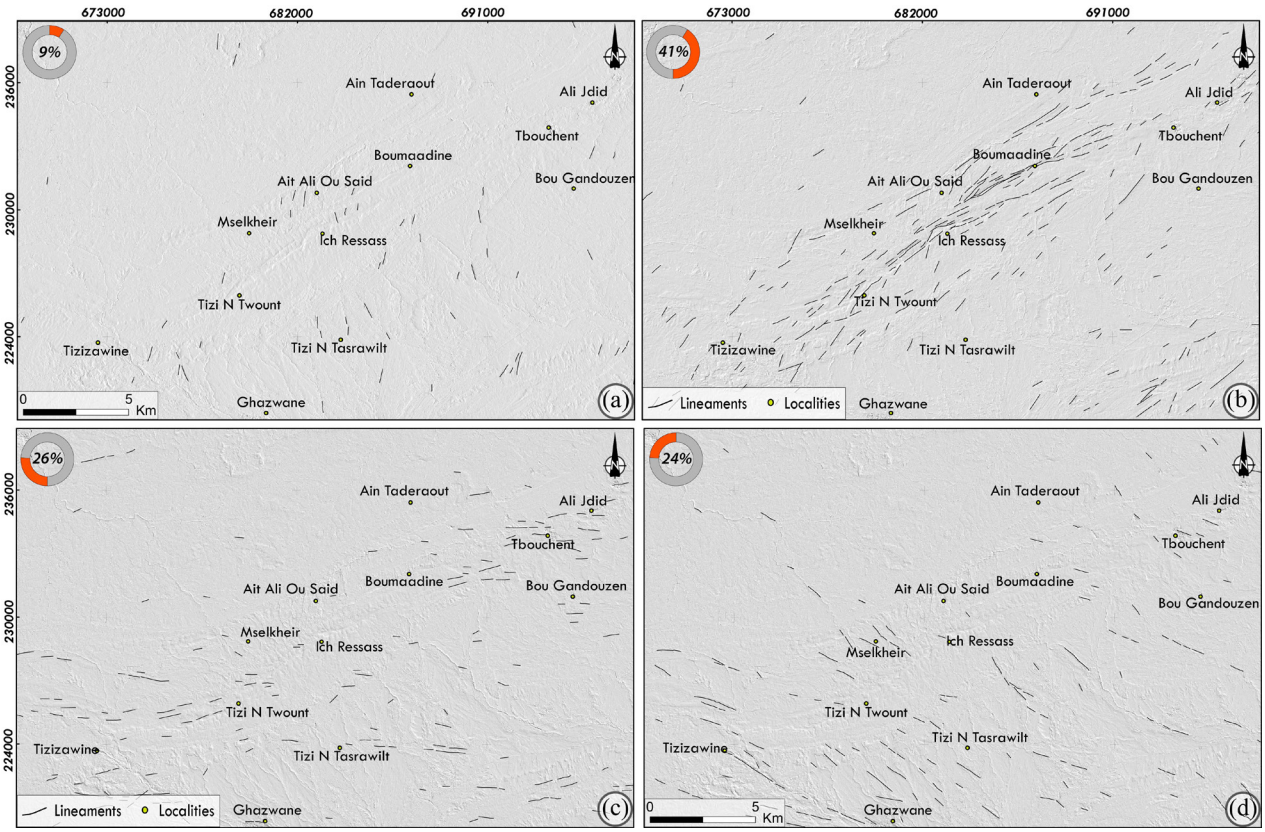

Figure 8.— Lineaments extracted from directional filters. (a) N-S lineaments. (b) NE-SW lineaments. (c) E-W lineaments. (d) NW-SE lineaments.

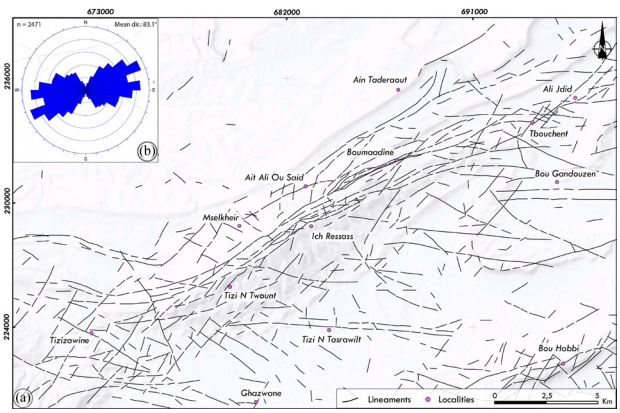

Figure 9.— (a) Synthetic map of fractures. (b) Rose diagram of the fracture's orientation.

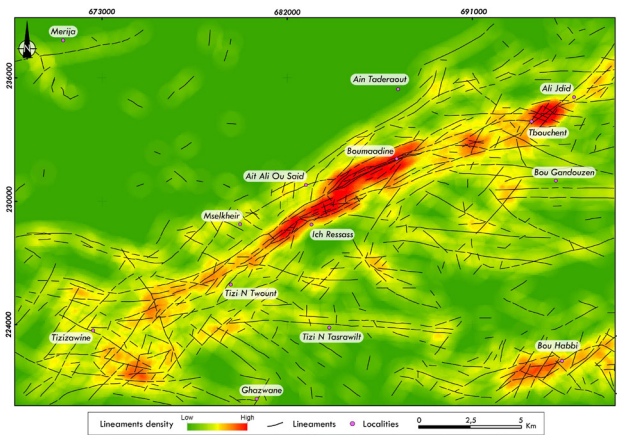

Figure 10.— Lineament density map.

Data integration

The superposition of satellite processing data (lineaments and alteration zones) (Figure 11) shows a perfect correlation between the high lineament density area (strong fracturing), the gossans and the hydrothermally altered zones. The resulting image shows that the anomalies are preferentially oriented ENE-WSW to NE-SW and located along the axis of Jbel Skindis and at Bou Habbi Area.

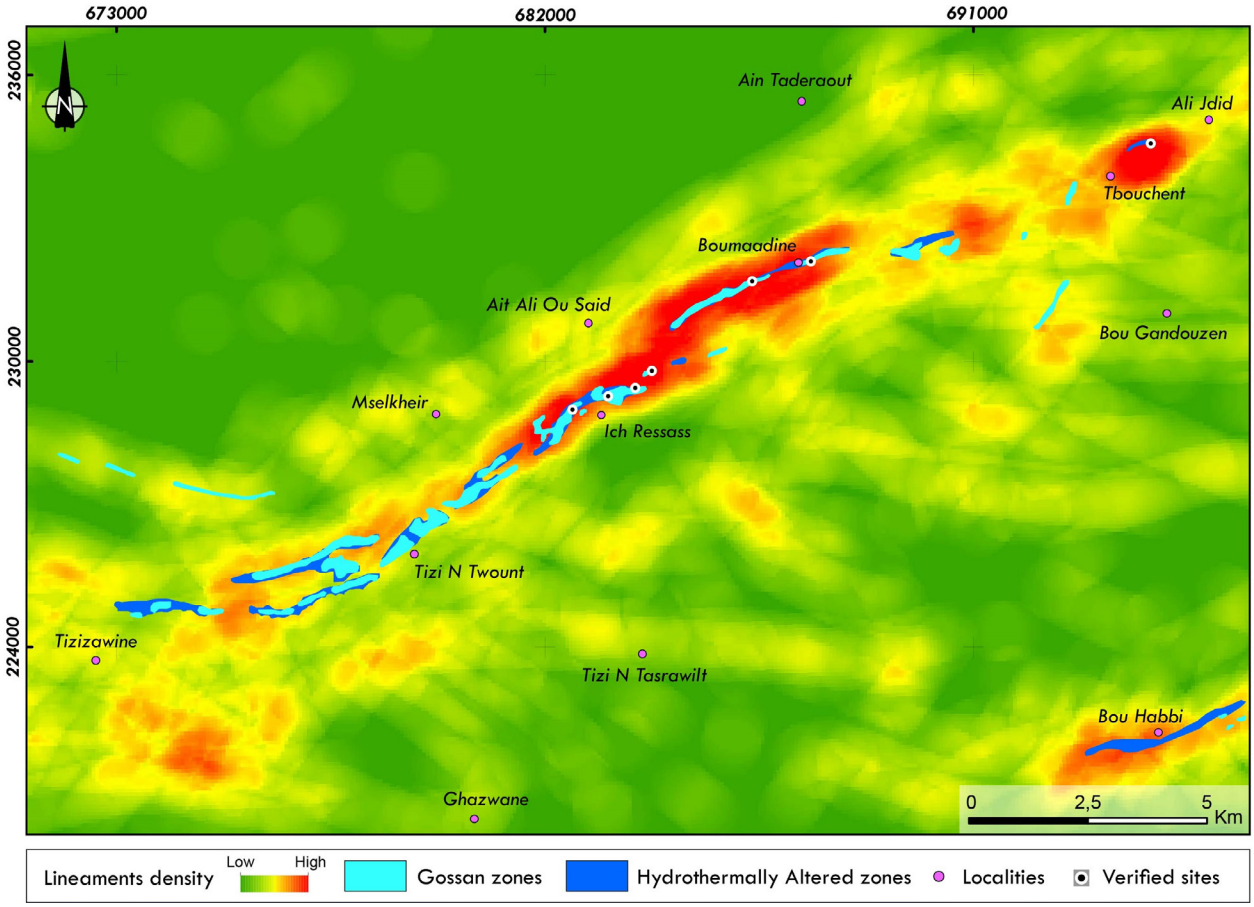

Figure 11.— Superposition of lineament density and mineral alteration maps.

Field verification

Field survey was conducted to verify the occurrence of mineralization in the anomalous areas. The results show some potential sites identified in the altered zones along the Jbel Skindis anticlinal hinge, and confirm the interpreted remote sensing imagery (Figure 11). Hematitization, dolomitization, gossans and iron oxides veins were found along anomaly zones (Figures 12A, 12B, 12C & 12E), these later showed some surface expression of goethite, hematite, coronadite, galena, pyrite and calcite. Also, some old mine galleries were found in the alteration zones (Figure 12D). Most of the veins are N70 bearing direction with subvertical dipping and hosted by altered dolostones of Lower Jurassic. One of the six verified sites (Tbouchent) showed the presence of mineralized veins striking N-S, hosted in limestone and marls of Middle Jurassic age, and developing an alteration halo consisting of ankeritization of limestone (Figure 12C), those veins are found in a highly fractured area in satellite imagery.

Discussion

In this work, multiple sources of spectral data derived from Aster, Landsat 8 OLI and Sentinel 2A sensors were utilized for the exploration of Fe-Mn-Pb mineralization in the Jbel Skindis region, High Atlas, Morocco. Band ratios and PCA image processing techniques were used to produce thematic maps of fracturing and alteration minerals; these later were integrated in a GIS system for indicating the high prospective zones.

Band rationing is a remote sensing image processing technique that has been successfully carried out by many authors to detect hydrothermal alteration minerals associated with the carbonate-hosted

Figure 12.— Field photographs: (a) Gossan outcrop. (b) Massive calcite lens and oxides vein. (c) N-S striking vein in Tbouchent area. (d) Artisanal exploitation of N80 striking vein. (e) massive Fe-Mn-Pb vein.

deposits around the world (Molan & Behnia, 2013; Yang *et al*., 2018; Sekandari *et al*., 2020; Ghorbani *et al*., 2019; Traore *et al*., 2022). Dolomitization, Ankeritization, hematitization and limonitization and supergene weathering are the main alteration types associated with the carbonate replacement deposit mineralization in the Jbel Skindis area, the spatial distribution of those alteration minerals was comprehensively mapped based on spectral characteristics of iron bearing minerals. A proposed Landsat 8 OLI greyscale image ratio 5/4 was used for mapping gossan zones which are rich of ferric oxides. this ratio allowed also highlighting the green vegetation scattered in the study area, this is due to the higher reflectance of the vegetation in the near-infrared (NIR) wavelength (Mancino *et al*., 2020). The false color composite (4/6, 2/1, 3/2) of Aster helps identifying the surface distribution of iron rich hydrothermal alteration.

The lineaments can be extracted from satellite images using both manual visualization (Sarp, 2007; Es-sabbar, 2020) and automatic extraction method through software such as PCI Geomatica (Koçal *et al*., 2004; Ibrahim & Mutua, 2014, Benaissi *et al*., 2022). A combination of manual and automatic extraction of lineaments by El-Sawy *et al*., (2016), deduced that the best way to identify the lineaments is the correlation between the lineaments extracted by both manual & automatic techniques. In this study, the lineaments that represent geological structures

like faults and fractures were considered important indicators of hydrothermal fluid circulation, hence controlling mineralization in the study area. Herein, the Landsat proposed false color composite (4, 6, 7) allows highlighting the structural and geomorphological features in the image, which helps us carrying out the visual interpretation and manual mapping of lineaments. The automatic extraction performed on the PC2 band of the sentinel 2A data shows a good performance in revealing lineaments that haven't been mapped by visual interpretation. Combining Sentinel and Landsat 8 OLI revealed maximum of lineaments affirmed significative in geological interpretation, and helped drawing a synthetic map of fracturing that can be used afterwards in exploring resources such as groundwater, oil and gas. The results obtained show the efficiency of combining the automatic extraction and the conventional manual method in mapping and characterization of lineaments at regional scale using Landsat and sentinel data.

Data integration showed that the mapped alteration minerals display a significant spatial correlation with areas of medium to high lineament density; their direction follows the main orientation of the lineaments identified in the study area. This result confirms the structural control of the alterations by the fracture networks.

Field verification was conducted in some anomalous zones by observing surface expression of Mn-Fe-Pb mineralization and related lithological units and alteration zones. Hematitization, ankeritization and gossans were found with the expression of lead and manganese oxides (coronadite, magnetoplumbite, hematite and goethite) and minor amount of calcite and sulfides (galena, chalcopyrite and pyrite). The manifestation of Pb-Mn-Fe mineralization was typically recorded in faults and fractured zones in the limestone and dolostones of Lower and Middle Jurassic. Based on those results, the prospective zones to be explored in the study zone are the NE oriented axis of Jbel Skindis and the Bou Habbi area.

Conclusions

The Processing of Landsat 8 OLI, Aster, and Sentinel 2A satellite data contributed fully to the mapping of alteration zones, and structural discontinuities in the Jbel Skindis (375 Km^2). The multicriteria analysis of these data in GIS tool checked by field observations, allowed orienting mining exploration by setting up regional prospecting guides for Mn-Fe-Pb mineralization.

The extraction of lineaments from Sentinel and Landsat images allowed the mapping of the main structural discontinuities in the study zone. Gossans and hydrothermal minerals, extracted from Aster and Landsat images, show that the anomalies are oriented NE-SW to ENE-WSW, and preferentially located on the axis of Jbel Skindis. Crossing of lineament data and alteration anomalies map with field data showed that the prospective zones are intimately linked to the highly fractured areas, characterized by gossans and iron rich hydrothermal alteration, and preferentially located in dolostone of Lower and Middle Jurassic age.

Therefore, the most favorable zones for possible tactical mining exploration of Mn-Fe-Pb mineralization in the study zone are the NE oriented axis of Jbel Skindis and the Bou Habbi area.

The results of this work show the effectiveness of remote sensing multi-sensor data processing coupled with GIS system integration, in lineament and alteration mineral mapping. The approach used in this work provides a model for future prospecting efforts for similar mineralization in the Eastern High Atlas, especially in inaccessible areas to help rapidly delineate mineral deposits at the surface.

ACKNOWLEDGMENTS

We would like to thank Africorp Mining Company, from "Africorp Consortium group", for their help and support throughout the course of this work. Additionally, we would like to express our appreciation to Mr. Luc Barbanson for revising the manuscript and for his valuable remarks.

REFERENCES

Atapour, H. & Aftabi, A. (2007). The geochemistry of gossans associated with Sarcheshmeh porphyry copper deposit, Rafsanjan, Kerman, Iran: Implications for exploration and the environment. Journal of Geochemical Exploration, 93: 47-65. https://doi.org/10.1016/j.gexplo.2006.07.007

Başıbüyük, Z. & Ekdur, E. (2018). Determination of iron minerals with landsat ETM, Kırşehir, Turkey. Gospodarka Surowcami Mineralnymi, 34: 23-36.

Benaissi, L.; Amraoui, T.; Tobi, A.; Ibouh, H.; Zaid, K.; Elamari, K. & Hibti. M. (2022). Geological mapping and mining prospecting in the Aouli inlier (Eastern Meseta, Morocco) based on remote sensing and geographic information systems (GIS). China Geology. https://doi.org/10.31035/cg2022035

Bouabdellah, M. & Sangster, D. (2016). Geology, Geochemistry, and Current Genetic Models for Major Mississippi Valley-Type Pb-Zn Deposits of Morocco. In: Mineral Deposits of North Africa (Bouabdellah, M. & Slack, J.). Mineral Resource Reviews, Springer, Cham, 463-495. https://doi.org/10.1007/978-3-319-31733-5_19

Bouchta, R. (1967). Étude géologique et micropaléontologique au Jbel Mechkakour (Haut Atlas oriental). PhD Thesis, Faculty of Sciences, Paris, 99 pp.

Caïa, J. (1969). Les minéralisations plombo-cupro-zincifères stratiformes de la région des plis marginaux du Haut Atlas oriental: un exemple de relations entre des minéralisations et une sédimentation détritique continentale: Maroc. Service Géologique Notes, 29: 107-120.

Caïa, J. (1976). Paleogeographical and Sedimentological Controls of Copper, Lead, and Zinc Mineralizations in the Lower Cretaceous Sandstones of Africa. Bulletin of the Society of Economic Geologists, 71: 409-422. https://doi.org/10.2113/gsecongeo.71.2.409

Choulet, F.; Charles, N.; Barbanson, L.; Branquet, Y.; Sizaret, S.; Ennaciri, A. & Chen, Y. (2014). Non-sulfide zinc deposits of the Moroccan High Atlas: multi-scale characterization and origin. Ore Geology Reviews, 56: 115-140. https://doi.org/10.1016/j.oregeorev.2013.08.015

Dresnay, R. (1963). La stratigraphie du Jbel Mechkakour (Hauts-Plateaux du Maroc oriental). Compte rendu sommaire des Séances de la Société géologique de France, Paris, fasc, 7: 238-240.

Drusch, M.; Del Bello, U.; Carlier, S.; Colin, O.; Fernandez, V.; Gascon, F.; Hoersch, B.; Isola, C.; Laberinti, P.; Martimort, P.; Meygret, A.; Spoto, F.; Marchese, O.S.F. & Bargellini, P. (2012). Sentinel 2: ESA's Optical High-Resolution Mission for GMES Operational Services. Remote Sensing of Environment, 120: 25-36. https://doi.org/10.1016/j.rse.2011.11.026

Duda, K.; Daucsavage, J.; Siemonsma, D.; Brooks, B.; Oleson, R.; Meyer, D. & Doescher, C. (2015). Advanced spaceborne thermal emission and reflection radiometer (aster) level 1 precision terrain corrected registered at-sensor radiance product (ast_l1t). US Geol Surv, USA.

El-Sawy, E.K.; Atef, M.I.; El-Bastawesy, A.M. & El-Saud, A.W. (2016). Automated, manual lineaments extraction and geospatial analysis for Cairo-Suez district (North-eastern Cairo-Egypt), using remote sensing and GIS. International Journal of Innovative Science, Engineering & Technology, 3(5): 491-500.

Emberger, A. (1965). Caractères polygénétiques des minéralisations plombifères de la Haute Moulouya (gisements d'Aouli, Mibladen et Zeïda, Maroc). Comptes Rendus Academie Sciences Paris (a), 260(9): 3433-3436.

ERDAS (Firm). (2007). ERDAS Field Guide. Leica Geosystems GIS & Mapping, LLC. Norcross. 378 pp.

Es-sabbar, B.; Essalhi, M.; Essalhi, A. & Si Mhamdi, H. (2020). Lithological and Structural Lineament Mapping from Landsat 8 OLI Images in Ras Kammouna Arid Area (Eastern Anti-Atlas, Morocco). Economic and Environmental Geology, 4: 425-440.

Essalhi, M.; Sizaret, S.; Barbanson, L.; Chen, Y.; Lagroix, F.; Demory, F.; Nieto, J.M.; Sáez, R. & Capitán, M.A. (2011). A case study of the internal structures of gossans and weathering processes in the Iberian Pyrite Belt using magnetic fabrics and paleomagnetic dating. Mineralium Deposita, 46: 981-999. https://doi.org/10.1007/s00126-011-0361-8

Ghorbani, A.; Honarmand, M.; Shahriari, H. & Hassani, M.J . (2019). Regional scale prospecting for non-sulphide zinc deposits using ASTER data and different spectral processing methods. International Journal of Remote Sensing, 40(23): 8647-8667. https://doi.org/10.1080/01431161.2019.1620372

Haddoumi, H. (1998). Les formations détritiques «couches rouges» (Bathonien et Crétacé inférieur) de la région d'Anoual (Haut Atlas oriental, Maroc): sédimentologie, stratigraphie et paléogéographie. PhD Thesis, Mohammed 1st University, Oujda, 229 pp.

Haddoumi, H.; Baidder, L.; Karim, M.; Kaoukaya, A.; Soulaimani, A.; Ouanaimi, H.; Amhoud, H.; Boudad , L.; Eddebbi, A.; Hilali, M.; Badra, L.; Mahmoudi, A.; El Arabi, E.H. & Allouban, M. (2018). Carte géologique du Maroc (1/50.000), Feuille Mazzer. Notes et Mémoires Serv. Géol. Maroc, 596.

Haddoumi, H.; Baidder, L.; Karim, M.; Ouanaimi, H.; Soulaimani, A.; Aria, E.H.; Kaoukaya, A.; Ettachfini, E.M.; Hafid, A.; Boudad , L.; Amhoud, H.; El Arabi, E.H.; Eddebbi, A.; Hilali, M. & Chibani, B. (2019). Carte géologique de Maroc (1/50 000), feuille de Talsint Ouest. Notes et Mémoires, Service Géologique Maroc, 607.

Hung, L.Q.; Batelaan, O. & De Smedt, F. (2005). Lineament extraction and analysis, comparison of Landsat ETM and Aster imagery. Case study: Suoimuoi tropical karst catchment. Vietnam. Proceedings SPIE 5983, Remote Sensing for Environmental Monitoring, GIS Applications and Geology V, Bruges, Belgium, 182-193. https://doi.org/10.1117/12.627699

Ibrahim, U. & Mutua, F. (2014). Lineament extraction using landsat 8 (OLI) in Gedo. Somalia. International Journal of Science and Research, 3(9): 291-296.

Ihlen, V. (2019). Landsat 8 (L8) Data Users Handbook, U.S. Geological Survey, LSDS-1574 Version 5.0, Ed.; USGS: EROS, Sioux Falls, South Dakota, 106 pp.

Jébrak, M. (2008). Géologie des ressources minérales. Ministère des Ressources Naturalles et de la Faune, Denis L. Lefebvre, 673pp.

Khunsa, F.; Ur Rehman, A.; Khattak, U.; Kausar, A.; Toqeer, M. & Haider, N. (2017). Minerals identification and mapping using ASTER satellite image. Journal of Applied Remote Sensing, 11(4): 046006. https://doi.org/10.1117/1.JRS.11.046006

Koçal, A.; Duzgun, H.S. & Karpuz, C. (2004). Discontinuity mapping with automatic lineament extraction from high resolution satellite imagery. ISPRS XX, Istanbul, 12-23.

Mancino, G.; Ferrara, A.; Padula, A.; Nolè, A. (2020). Cross-Comparison between Landsat 8 (OLI) and Landsat 7 (ETM+) Derived Vegetation Indices in a Mediterranean Environment. Remote Sens, 12: 291. https://doi.org/10.3390/rs12020291

Mattauer, M.; Tapponier, P. & Proust F. (1977). Sur les mécanismes de formation des chaînes intracontinentales. L'exemple des chaînes atlasiques du Maroc. Bulletin de la Société géologique de France, 7: 521-526. https://doi.org/10.2113/gssgfbull.S7-XIX.3.521

Molan, Y.E. & Behnia, P. (2013). Prospectivity mapping of Pb-Zn SEDEX mineralization using remote-sensing data in the Behabad area, Central Iran. International journal of remote sensing, 34(4): 1164-1179. https://doi.org/10.1080/01431161.2012.718460

Mouguina, E.M. (2004). Les minéralisations polymétalliques (Zn-Pb, Cu, Co, Ni) du Jurassique du Haut Atlas central (Maroc) : Contexte géodynamique, typologies et modèles génétiques. PhD Thesis, Faculty of Sciences, Marrakech, 320 pp.

Piqué, A. & Michard, A. (1989). Moroccan Hercynides: a synopsis. The Paleozoic sedimentary and tectonic evolution at the northern margin of West Africa. American Journal of Science, 289: 286-330. https://doi.org/10.2475/ajs.289.3.286

Pour, A.B.; Hashim, M. & Marghany, M. (2010). Characterization of ASTER Data for Mineral Exploration. Proceedings of the MRSS 6th international remote sensing & GIS conference and exhibition, Kuala Lumpur, Malaysia, 6.

Prost, G.L. (2013). Remote sensing for geoscientists. Third Edition (3rd Ed.). CRC Press. https://doi.org/10.1201/b15638

Rajendran, S.; Thirunavukkarasu, A.; Balamurugan, G. & Shankar, K. (2011). Discrimination of iron ore deposits of granulite terrain of Southern Peninsular India using ASTER data. Journal of Asian Earth Sciences, 41(1): 99-106. https://doi.org/10.1016/j.jseaes.2011.01.004

Rouvier, H.; Perthuisot, V. & Mansouri, A. (1985). Pb-Zn deposits and salt-bearing diapirs in Southern Europe and North Africa. Economic Geology, 80(3): 666-687. https://doi.org/10.2113/gsecongeo.80.3.666

Roy, D.; Wulder, M.; Loveland, T.; Woodcock, C.; Allen, R.; Anderson, M.; Helder, D.; Irons, J.; Johnson, D.; Kennedy, R.; Scambos, T.; Schaaf, C.; Schott, J.; Sheng, Y.; Vermote, E.; Belward, A.; Bindschadler, R.; Cohen, W.; Gao, F.; Hipple, J.; Hostert, P.; Huntington, J.; Justice, C.; Kilic, A.; Kovalsky, V.; Lee, Z.; Lymburner, L.; Masek, J.; McCorkel, J.; Shuai, Y.; Trezza, R.; Vogelmann, J.; Wynne, R. & Zhu, Z. (2014). Landsat-8: Science and product vision for terrestrial global change research. Remote Sensing of Environment, 145: 154-172. https://doi.org/10.1016/j.rse.2014.02.001

Sarp, G. & Toprak, V. (2007). Spatial analysis of lineaments, north-west of Ankara. 28th Asian Conference on Remote Sensing, ACRS, 3.

Scanvic J. 1993. Télédétection aérospatiale et informations géologiques. BRGM Manuels et méthodes, Orleans, 284 pp.

Sekandari, M.; Masoumi, I.; Muslim, A.; Rahmani, O.; Hashim, M.; Zoheir, B.; Pradhan, B.; Misra, A. & Aminpour, S. (2020). Application of Landsat-8, Sentinel-2, ASTER and WorldView-3 Spectral Imagery for Exploration of Carbonate-Hosted Pb-Zn Deposits in the Central Iranian Terrane (CIT). Remote Sensing, 12(8): 1239. ttps://doi.org/10.3390/rs12081239

Singh, A. & Harrison, A. (1985). Standardized principal components. International Journal of Remote Sensing, 6: 883-896. https://doi.org/10.1080/01431168508948511

Traore, M.; Çan, T. & Tekin, S. (2022). Mapping carbonate-hosted Pb-Zn mineralization zones in Yahyali Province (Eastern Taurus-Turkey) using ASTER data. Advances in Space Research, 69(1): 266-281. https://doi.org/10.1016/j.asr.2021.07.034

Yang, M.; Ren, G.; Han, L.; Yi, H. & Gao, T. (2018). Detection of Pb-Zn mineralization zones in west Kunlun using Landsat 8 and ASTER remote sensing data. Journal of Applied Remote Sensing, 12(2): 18-26. https://doi.org/10.1117/1.JRS.12.026018

Younis, M.T.; Gilabert, M.A.; Melia, J. & Bastida, J. (1997). Weathering process effects on spectral reflectance of rocks in a semi-arid environment. International Journal of Remote Sensing, 18(16): 3361-3377. https://doi.org/10.1080/014311697216928